Nuclear Instruments and Methods in Physics Research B xxx (2014) xxx–xxx

Contents lists available at ScienceDirect

Nuclear Instruments and Methods in Physics Research B

journal homepage: www.elsevier.com/locate/nimb

Evaluation of a setup for pNRA at LIBAF for applications in geosciences

M. Borysiuk *, P. Kristiansson, L. Ros, N. Abdel, M. Elfman, E.J.C. Nilsson, J. Pallon

Division of Nuclear Physics, Department of Physics, Lund University, Box 118, SE-221 00 Lund, Sweden

ARTICLE INFO

Article history:
Available online xxxx

Keywords:
IBA
NRA
Isotopes
Coincidence

ABSTRACT

A new setup for photon tagged nuclear reaction analysis pNRA is being developed at Lund's ion beam analysis facility LIBAF. Particle induced gamma ray emission PIGE and nuclear reaction analysis NRA are two methods that have been extensively used for light isotope measurement in ion beam analysis IBA. There is an abundance of nuclear reactions between light elements and MeV protons, deuterons and alpha particles. This means that in principle all elements from lithium all the way up to chlorine can be analyzed using those techniques. Detection limits can be improved for some elements, if those two methods are fused together into pNRA.

The new setup for pNRA will benefit from advances in detector technology that occurred during the last 20 years. A $LaBr_3$ scintillator detector and an annular double sided silicon strip detector DSSSD are used in coincidence to detect a gamma and a charged particle respectively. Both detectors are connected to a VME based data acquisition system. Of primary interest in this work is the analysis of isotopic ratios of light elements in geological samples, which are usually thick with a complex matrix. This setup can be for instance used to measure isotopic fractionation of oxygen and boron. We will present the setup and discuss its capabilities.

1. Introduction

There is a multitude of methods available within ion beam analysis IBA [1]. A new setup for photon tagged nuclear reaction analysis pNRA [2] is currently under development at Lund's ion beam analysis facility LIBAF. pNRA combines Particle Induced Gamma ray Emission PIGE and Nuclear Reaction Analysis NRA into one technique. Those two aforementioned methods have been extensively used for light isotope spectroscopy in IBA [3]. The principle of pNRA is to analyze isotopic content of a sample by detecting both the gamma quanta and the charged particle produced in a nuclear reaction [4]. This technique was first proposed 20 years ago, it was suggested that it could be used for trace element analysis in thin samples [2] and depth profiling of thick samples [5].

The availability of many nuclear reactions for interaction of light ions with matter means that with the right choice of projectile and projectile energy all elements from lithium all the way up to chlorine can be observed and quantified [6]. Previous pNRA setup at LIBAF has been used for boron measurements in biological samples [7]. It was also suggested that this method could be successfully combined with a nuclear microprobe setup [6]. Important for this study is that pNRA can be used to measure isotopic fractionation of light elements.

The primary goal for the new setup is the analysis of geological material, which entails thick samples with a complex matrix. Isotopic fractionation of light elements is relevant in many contexts within geosciences. The application that inspired the current project is stable oxygen isotope quantification in extraterrestrial geological material. Oxygen isotopic fractionation can be used to both recognize and classify the extraterrestrial minerals [8]. In complex thick and semi-thick samples background and interferences can be a problem for PIGE and NRA. Here pNRA can prove to be superior [6].

2. Method

The minimum equipment required for pNRA is a source of MeV ions, a particle detector, a gamma detector and electronics for creating a coincidence [2]. The tagging of the charged particle with the corresponding gamma is a way of suppressing the background and separating the interesting reactions from interferences expected in complex targets. The interesting nuclear reactions in this case are inelastic scatterings and resonances, which leave the nucleus in an excited state, so that γ-emission is possible.

The setup discussed in the current work benefits greatly from advances in detector technology that occurred during the last few decades. Description of the old setup can be found in [6]. This

* Corresponding author. Address: Fysiska institutionen Box 118, 221 00 LUND HS:14, Sweden. Tel.: +46 46 22 27733.
E-mail address: maciek.borysiuk@nuclear.lu.se (M. Borysiuk).

http://dx.doi.org/10.1016/j.nimb.2014.02.061
0168-583X/

new setup was installed and tested at LIBAF, which is a facility based around a single ended 3 MV accelerator of Van der Graff type with a nuclear microprobe and p, d and α beams [9].

The ability to capture as large as possible fraction of reaction products is always desirable in Nuclear Physics. This is especially true here since the limiting factor for the detection of each element is the cross sections of the nuclear reactions involved; many of those are on the order of some mb [1]. For the charged particle this means primarily large solid angle coverage is desired. Due to slow integration times for standard shaping electronics and large cross section for elastic scattering, the ability to suppress or prevent pile-up is also highly desirable. For the gamma particles the relevant parameter to maximize the yield is the gamma capture efficiency, which is related to both the detector size and the scintillator material. In simple terms an efficient pNRA experiment requires large detectors and a compact geometry. Other important parameters for this kind of setup are a good timing and a good energy resolution. Improving those greatly improves background suppression which means a gain in signal to noise ratio.

3. Experiment

Fig. 1 provides a schematic description of the experimental setup. The detectors used are a large 1.5 × 2 inches cylindrical $LaBr_3$ scintillator detector [10] and a double sided silicon strip detector DSSSD, previously described in [11]. They are used in coincidence to detect a gamma and a charged particle respectively. The analog electronics on the DSSSD side consists of Mesytec preamplifier MPR-16 and shaper STM-16 [11,12]. Shaping amplifiers provide both the energy and timing signals. Signals from the PMT can be used without amplification and split to provide both timing and energy. The rest of the analog electronics is a standard coincidence setup constructed out of NIM modules. The only complication is aligning the timing of gamma and particle signals to create a common gate for both of them in the data acquisition system DAQ. Passive delay cables are used for that purpose. The faster, gamma branch starts the coincidence. A 1 μs long coincidence gate is used, which is more than enough to observer all, prompt and nearly prompt reactions. The shorter gate allows us to increase current and get stronger signal for the same background. In principle a TOF of less than 5 ns is expected between the gamma start and particle stop, for prompt particles. In reality the leading edge discriminators built into the shaping electronics on the DSSSD introduce an amplitude walk into the spectrum [13]. The setup is very flexible since there is always the option of switching the coincidence off which reduces the method back to PIGE, RBS and NRA.

$LaBr_3$ is a new scintillator material intended for applications where both the timing and energy resolution are important. This inorganic crystal has density of 5.3 g/cm^3, which is more than NaI, CsI and BaF_2. That means it has a higher absorption efficiency then all three of them [14]. This material has a very good energy resolution (3% @ 660 keV) and timing properties (250 ps pulse rise time) [14]. The Hamamatsu PMT attached to this particular detector is fast, small and vacuum compatible, which means that the detector can be placed in the reaction chamber, less than 1 cm behind the target. The count rate in the gamma detector is nowhere near enough to saturate the detector, so as compact as possible geometry is desired. In this geometry the solid angle of the detector is 3.6 sr.

The DSSSD is placed 3 cm in front of the target. This DSSSD is annular with 64 radial electrodes on the front side and 32 ring shaped electrodes on the back side of the detectors as described in [11]. A real particle is defined as an event that generates equal amount of charge in two electrodes, one on the front and one on the backside of the detector, this means there are 2048 possible pixels. This large segmentation removes the pileup and adds angular information, which can be further used to separate interesting reactions. This version of DSSSD has an inner active diameter of 14 mm, active outer diameter of 85 mm and a dead layer of 2 μm. For the current geometry the size of the detector is 2.5 sr, each individual pixel is on the order of 1 msr.

Together those two detectors have large solid angle coverage for both the particle and the gamma quanta. The true coincidence rate for this system will be defined by the smallest detector or rather smallest solid angle times interaction efficiency which is almost 100% for a particle detector and which is an energy dependent quantity for the gamma detector.

The main drawbacks of the system are the internal activity of the $LaBr_3$ crystal, which leads to a characteristic spectrum seen in Fig. 2 (dotted line). This activity is due to decay of ^{138}La, a naturally occurring La isotope, and due to contamination of the crystal with ^{227}Ac, which is part of actinium series decay chain [10]. The

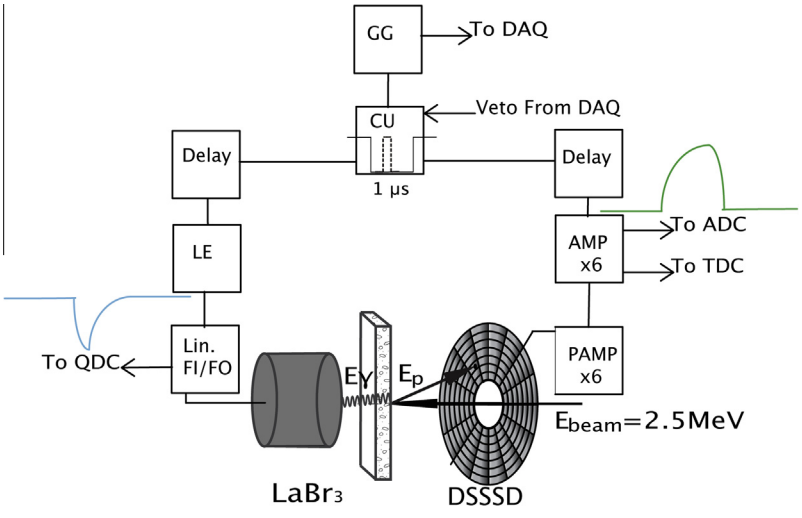

Fig. 1. Experimental setup consists of a large area segmented particle detector, DSSSD and a fast gamma detector, a $LaBr_3$ scintillator. DSSSD is placed in the backward geometry, $LaBr_3$ in the forward geometry, both detectors capture large portion of the solid angle. Coincidence setup is built out of standard NIM electronics. Scintillator energy output is split and used to generate start for the coincidence gate of 1 μs length. Triggers from the silicon shapers are used as the stop signals. It is necessary to introduce delay to get both energy signals into the gate.

Please cite this article in press as: M. Borysiuk et al., Evaluation of a setup for pNRA at LIBAF for applications in geosciences, Nucl. Instr. Meth. B (2014), http://dx.doi.org/10.1016/j.nimb.2014.02.061

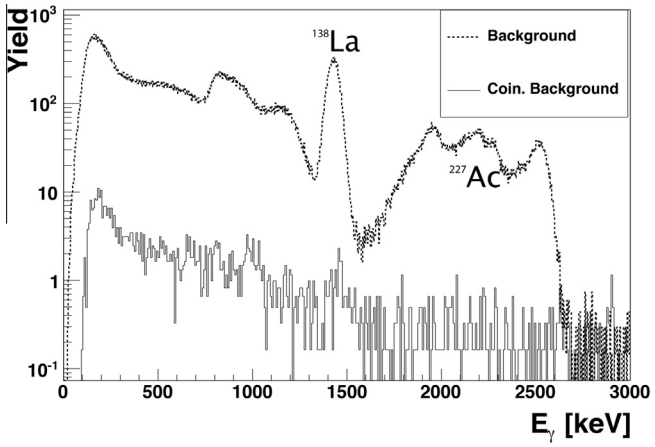

Fig. 2. The dotted line is a spectrum taken with the scintillator, shielded in lead housing. The internal activity of $LaBr_3$ [10] gives rise to this characteristic background. This data is normalized to 1000 s. The observed lines come partially from the decay of ^{138}La, which is a naturally occurring isotope of La, and partially from contamination present in the crystal in the form of ^{227}Ac, which belongs to actinium decay chain. The solid line is the activity observed in a coincidence with elastically scattered protons from a thick blank target bombarded with 1 nA proton beam, data is normalized to charge of 1 μC. The solid line is the rate of accidental coincidences and it should have the same structure as the dotted line, only scaled down by the coincidence gate length and the rate of elastically scattered particles.

magnitude of the activity varies between crystals, primarily depending on their size. The internal activity places a limit on the minimum yield that must be generated by a given resonance so that it can be seen. This directly affects the minimum detectable limit for each element, depending on the resonances available and on the overall sample composition. In Fig. 2 (solid line) a coincidence spectra from a thick metal sample where no true coincidences are expected is normalized to 1 μC. Here only a few counts per keV are seen for energies above 200 keV so the background for resonances occurring at higher gamma energies should be negligible for all strong nuclear reactions. The higher background at lower energies should be at least partially compensated by the nearly 100% gamma absorption efficiency of the detector at those energies. On the particle side segmented detector requires more attention than a regular planar particle detector since it has 96 electronics channels. All of which have to be adjusted individually. Because of the large size of the detector, whenever exact energies of particles are required detector dead layer and experimental geometry has to be considered since they will have a measurable effect on the experimental results [15].

The detectors are connected to a VME based DAQ. It includes 3 peak shaping ADC modules v785 for reading out the DSSSD, a QDC module v792 for the PMT energy signal and a multihit TDC module v1290N for timing information, all designed and built by CAEN [16]. Proton charge is measured in the off-axis Faraday cup before the target. The beam is deflected into the cup with a frequency of 10 Hz, and converted to digital pulses with a charge to frequency converter, as described in [17]. The version of the DAQ used in the current experiment was limited to some 3000 events per second. Gathered data was stored and evaluated using a ROOT [18] based analysis program. The capacity of the DAQ was not a limiting factor in the current experiment since due to the hardware coincidence condition the count rate was below 300 counts per second. Observably the dead time during the experimental run was on the order of 2%. The acquisition system currently in development should be able to handle the data rates that are at least an order of magnitude higher. For the types samples considered here and currents available at LIBAF that should be sufficient.

4. Results

To evaluate the systems performance data has been taken for some representative samples. The event mode data acquisition provides us with three correlated parameters for each event that are used to find and isolate interesting reactions. The parameters are the energies of the particle and of the gamma quanta, and their relative arrival time at their corresponding detectors. This information can be combined into a number of figures commonly used in coincidence experiments. The timing information gives the coincidence peak, which is used as the main filtering condition in a coincidence experiment. The plot of energies of the entities involved in the coincidence gives a two-dimensional energy–energy plot. This plot provides an immediate identification and separation of the interesting reactions.

The focused proton beam at 2.5 MeV was scanned over the samples. Materials used as test samples were thin PIXE standards originally intended for calibration of a PIXE or an XRF setup [19]. They each consist of 2 μm Mylar backing with known amounts of the element of interest deposited onto them. Since the intended target for the system are thick geological samples, those standards were fixed onto a thick brass backing. The sample materials were CaF_2, NaCl and Al. This sample configuration is intended to approximate real physical situation, at least as far as background level is concerned.

In Fig. 3 reactions induced in CaF_2 sample are studied. A reaction marked as D in the figure is ^{19}F(p,pγ) ^{19}F for E_γ = 197 keV [20] and is an interesting case to observe. This reaction is a nearly prompt decay for which the decay time is slow enough to measure. The previously measured half-life of this transition is 90 ns and this value can be easily recreated from the projection of the figure onto the time axis. A truly prompt ^{19}F(p, αγ)^{16}O marked as P can be seen as well, this reaction is induced above a number of high lying levels in the ^{16}O nucleus which means that several strong gamma rays can be observed when a cut is placed on this reaction [21].

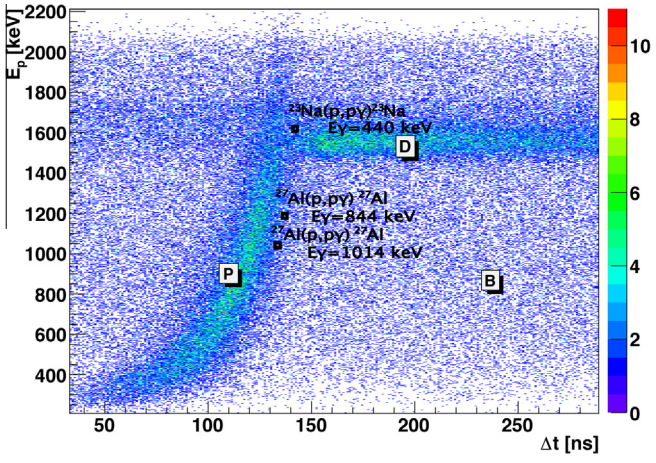

Fig. 3. The particle energy is plotted as function of coincidence time for the CaF_2 sample bombarded with 2.5 MeV protons. The prompt coincidences marked with P in the figure are energy dependent. This is due to leading edge discriminators built into the shaping amplifiers. This type of signal pickoff suffers from a well-known amplitude walk [13]. The cut placed around the prompt distribution reveals that those events are correlated with a ^{19}F (p, αγ)^{16}O reaction, which has several gammas between 6 and 7 MeV. The structure marked with D in the figure belongs to a delayed reaction ^{19}F(p,pγ) ^{19}F reaction which has a measurable decay time of 90 ns and a gamma decay energy of 197 keV. Rest is B, background and when projected onto gamma energy axis shows the same structures as the two spectra in Fig. 2. It is interesting to compare this data with other samples, specifically ones with prompt inelastically scattered protons. Three such reactions have been observed during this experiment. The positions those reactions would have in the current energy-time spectra are marked. They create a line shifted in time, parallel to the one created by prompt alpha particles.

Please cite this article in press as: M. Borysiuk et al., Evaluation of a setup for pNRA at LIBAF for applications in geosciences, Nucl. Instr. Meth. B (2014), http://dx.doi.org/10.1016/j.nimb.2014.02.061

A hardware coincidence condition with 1 μs long gate is used as the trigger for the data acquisition system, but this gate can be easily shortened to a few hundred nanosecond. Unfortunately the actual prompt coincidence peak in the timing spectrum without any further context would have rather poor time resolution. As can be seen in Fig. 3 projection of the prompt peak, marked as P, onto the time axis is more than 50 ns thick and clearly asymmetric. Thus extending coincidence time spectra into a two dimensional histogram, where the energy of the particle is plotted as the function of arrival time in each detector, is an important tool. This way we see that the coincidence time is not a straight line. It changes with the energy of the particle. This is a direct effect of the leading edge discriminators built into the shaping amplifiers. It is well understood that the leading edge timing circuits are affected by the energy of the signal [13]. This problem can be solved in hardware, for instance constant fraction discriminators do not suffer from that problem, but that would require additional investment in electronics. Making a banana shaped cut in the particle energy-time spectrum, which follows the behavior of the leading edge discriminators, is sufficient to separate the real coincidences from accidental background. The same cut was placed on each one of the timing spectra. Actual FWHM of timing peak when leading edge behavior is taken into account is less than 16 ns.

Positions of the three peaks observed in the energy-time spectra during the measurements on Al and Na rich samples have been superimposed onto the current spectrum. Those 3 processes are inelastic scattering reactions of protons and mark a line parallel to the one created by the $^{19}F(p,\alpha\gamma)^{16}O$ reaction. This suggests that it should be possible to separate protons from alpha particles with this setup.

An example of a particle-gamma energy spectrum can be seen in Fig. 4. A sample of NaCl was irradiated with 14.4 μC of protons. Two reactions can be clearly seen at the energy of 2.5 MeV. They are identified as $^{23}Na(p,p\gamma)\,^{23}Na$ with $E_\gamma = 440$ keV and $^{23}Na(p,\alpha\gamma)\,^{20}Ne$ with $E_\gamma = 1636$ keV [22]. Energy resolution of the $LaBr_3$ during this run was around 9% much worse than the expected 3%. This is most likely due to noise in analog electronics. Still both reactions can be clearly seen and separated. In Regular NRA experiment those two interactions would interfere with each other, which complicates the quantification. This is not a problem for pNRA. The stronger one of the two reactions is used to estimate minimum detectable limit for sodium.

Table 1
In the table the compilation of data for the analyzed samples is presented. Thin standard samples of Al, NaCl and CaF_2 were irradiated. Deposited charge was normalized to the system's dead time. Sensitivity S and minimum detection limit MDL were estimated for the current experimental settings. Both sensitivity and MDL vary 2 orders of magnitude, which is expected for this method. The measurement was done without any special consideration for any of the reactions and without scanning of the beam in energy in search of stronger resonance. Even so many reactions can be observed. Much better results could be easily obtained for each element by focusing on a specific reaction and resonance at the expense of some other reaction and isotope.

Sample	Charge (μC)	Sensitivity (counts/(μC ∗ μg/cm^2))	MDL ((μg/cm^2)/μC)
Na	14.4	145.6	0.36
F	12.7	20.9	4.84
Al	16.5	1.32	20

Compilation of the relevant results such as minimum detectable limit for the samples described above and for the Al standard can be found in Table 1. Cross section data for relevant reactions are available in the IBANDL database [23]. Minimum detectable limit depends on the background counts under the peak (N_b) and systems sensitivity (S), MDL = $3 * N_b/S$, where sensitivity S is yield per μC per amount of substance. It can be seen in the table that both of those numbers vary two orders of magnitude between the samples. That is an expected behavior for the pNRA method. They can also vary rather strongly with beam energy and detector geometry used. This means that these numbers can be improved for individual isotopes, but never for an entire range of elements simultaneously.

5. Conclusions

As was shown in figures and explained in the previous section almost background free spectra can be produced with straightforward cuts on the data. The standard samples with known areal concentrations used in the experiment allow us to estimate minimum detectable limit, for a number of elements, for the current experimental settings. The internal activity of the $LaBr_3$ detector is the primary factor defining the detection limit for most samples of interest, which will be thick with dense matrix, often consisting of heavy atoms. The accidental background seen is small and can

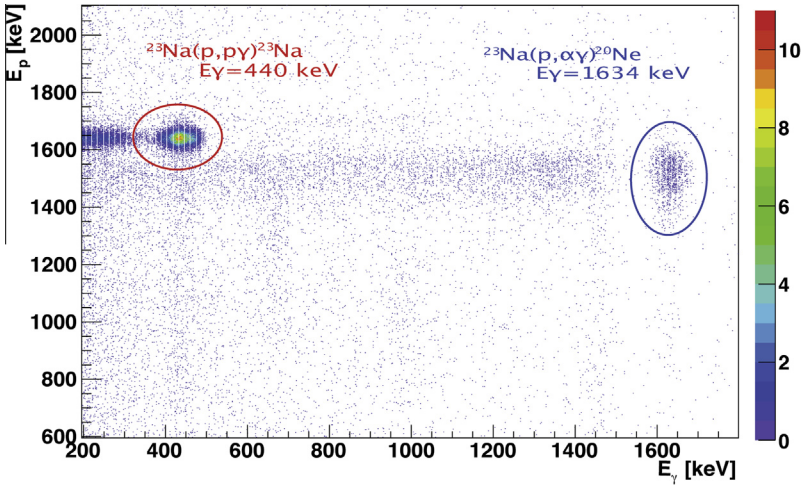

Fig. 4. Gamma energy versus particle energy for each valid event is plotted. A sample containing NaCl with known concentration was irradiated with 14 μC of protons at 2.5 MeV, two reactions between Na and protons can be clearly seen after the timing cut is placed on the prompt decay peak in the energy-time spectrum. A very strong peak belongs to $^{23}Na(p,p\gamma)\,^{23}Na$ with $E_\gamma = 440$ keV and a much weaker one to $^{23}Na(p,\alpha\gamma)\,^{20}Ne$ with $E_\gamma = 1636$ keV. Both can be used to extract information about sodium content in the sample. The first reaction provides much better sensitivity at least at this bombarding energy.

Please cite this article in press as: M. Borysiuk et al., Evaluation of a setup for pNRA at LIBAF for applications in geosciences, Nucl. Instr. Meth. B (2014), http://dx.doi.org/10.1016/j.nimb.2014.02.061

be decreased even further with a choice of a shorter coincidence gate.

pNRA is a method useful in specific situations only. It will not replace existing techniques but it can easily complement them. NRA and PIGE are both hampered by lack of cross section information together with errors in energy loss. This makes analysis of complex spectra difficult and often ambiguous. pNRA spectra by the very nature of this method promise to be cleaner with less background and fewer interferences, desired resonances can be studied with greater ease.

A more precise experimental run is necessary to fully determine the limitations of the system and account for them. The particular pNRA setup under construction at LIBAF could be potentially used to provide additional information. Position sensitivity of the DSSSD could be used as an additional criterion in data evaluation since the cross section of many resonances has a strong angular dependence. Even mass separation should in principle be attainable although this might require an investment in faster electronics. The next step for this setup is to apply it to a set of oxygen standard samples and real geological samples and measure oxygen content and isotopic ratio.

References

[1] Y. Wang, M. Nastasi (Eds.), Handbook of Modern Ion Beam Materials Analysis, 2nd ed., Materials Research Society, 2009.
[2] P. Kristiansson, E. Swietlicki, Nucl. Instrum. Methods B 49 (1990) 98–105.
[3] G. Amsel, W.A. Lanford, Ann. Rev. Nucl. Part. Sci. 34 (1984) 435–460.
[4] Per Kristiansson, Bengt G. Martinsson, Nucl. Instrum. Methods B 132 (1997) 159–176.
[5] H.D. Carstanjen, W. Decker, J. Diehl, Th. Enders, R.M. Emrick, A. Föhl, E. Friedland, D. Plachke, H. Stoll, Nucl. Instrum. Methods B 51 (1990) 152–162.
[6] P. Kristiansson, S. Al-Suhaili, M. Elfman, K.G. Malmqvist, J. Pallon, K.A. Sjöland, Nucl. Instrum. Methods B 136–138 (1998) 362–367.
[7] K.A. Sjöland, P. Kristiansson, P. Tallone, Nucl. Instrum. Methods B 104 (1995) 255–260.
[8] R.C. Greenwood, I.A. Franchi, J.M. Gibson, G.K. Benedix, in: 38th Lunar and Planetary Science Conference, League City, Texas, USA, 12–16 March 2007.
[9] A. Shariff, C. Nilsson, V. Auzelyte, M. Elfman, P. Kristiansson, K. Malmqvist, J. Pallon, M. Wegdén, Nucl. Instrum. Methods B 231 (2005) 7–13.
[10] F. Quarati, A.J.J. Bos, S. Brandenburg, C. Dathy, P. Dorenbos, S. Kraft, R.W. Ostendorf, V. Ouspenski, A. Owens, Nucl. Instrum. Methods A 574 (2007) 115–120.
[11] P. Golubev, P. Kristiansson, N. Artega-Marrero, M. Elfman, K. Malmqvist, E.J.C. Nilsson, C. Nilsson, J. Pallon, M. Wegden, Nucl. Instrum. Methods B 267 (2009) 2065–2068.
[12] <http://www.mesytec.com/silicon.htm> (retrieved 22.07.13).
[13] J.M. Puzović, I.V. Aničin, Nucl. Instrum. Methods Phys. Res. A 572 (2007) 926–928.
[14] P. Dorenbos, J.T.M. de Haas, C.W.E. van Eijk, IEEE Trans. Nucl. Sci. 51 (2004) 1289–1296.
[15] U.C. Bergmann, H.O.U. Fynbo, O. Tengblad, Nucl. Instrum. Methods Phys. Res. A 515 (2003) 657–664.
[16] <http://www.caen.it/csite/Product.jsp?parent=11&Type=Product> (retrieved 22.07.13).
[17] P. Kristiansson, M. Borysiuk, N. Arteaga-Marrero, M. Elfman, E.J.C. Nilsson, C. Nilsson, J. Pallon, Nucl. Instrum. Methods B 268 (2010) 1727–1730.
[18] R. Brun, F. Rademakers, Nucl. Instrum. Methods Phys. Res. A 389 (1997) 81–86.
[19] <http://www.micromatter.com> (retrieved 22.07.13).
[20] A.P. Jesus, B. Braizinha, J.P. Ribeiro, Nucl. Instrum. Methods Phys. Res. B 161–163 (2000) 186–190.
[21] F. Ajzenberg, T. Lauritsen, Rev. Mod. Phys. 24 (1952) 321–402.
[22] A. Caciolli, G. Calzolai, M. Chiari, A. Climent-Font, G. Garcia, F. Lucarelli, S. Nava, Nucl. Instrum. Methods Phys. Res. B 266 (2008) 1392–1396.
[23] <http://www-nds.iaea.org/ibandl/> (retrieved 22.07.13).

Please cite this article in press as: M. Borysiuk et al., Evaluation of a setup for pNRA at LIBAF for applications in geosciences, Nucl. Instr. Meth. B (2014), http://dx.doi.org/10.1016/j.nimb.2014.02.061